Nanoscale

Accepted Manuscript

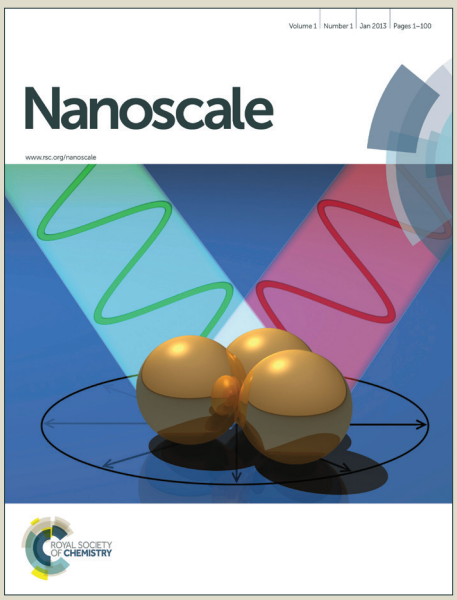

ROYAL SOCIETY OF CHEMISTRY

www.rsc.org/nanoscale

Cite this: DOI: 10.1039/c0xx00000x

www.rsc.org/xxxxxx

ARTICLE TYPE

Solution-Processed Flexible Transparent Conductors Based on Carbon Nanotubes and Silver Grids Hybrid

Jing Wang, Jintao Zhang, Ashok Kumar Sundramoorthy, Peng Chen* and Mary B. Chan-Park*

Received (in XXX, XXX) XthXXXXXXXXX 20XX, Accepted Xth XXXXXXXXX 20XX

DOI: 10.1039/b000000x

In a simple, cost-effective, and solution-based process, thin-film of single-walled carbon nanotubes is hybridized on a PET film which has been patterned with solution self-assembled Ag nanoparticles. Such flexible and transparent electrode exhibits sheet resistance down to ~5.8 Ω sq^{-1} at ~83.7% optical transmittance. The hybrid films are stable in ambient condition and offer excellent bendability.

Introduction

Transparent electrodes are critical components for many modern applications such as organic photovoltaics (OPVs), touch panels, organic light-emitting diodes (OLEDs), architectural windows and touch sensors. With increasing demand for cheaper but more sophisticated consumer electronics, there is ever-increasing demand for alternatives to current transparent conductive films. Currently, transparent conductors are usually made from doped metal oxides and among them, indium tin oxide (ITO) is the most commonly used material due to its high transparency and low resistance. However, ITO has several intrinsic drawbacks including resource shortage and rising price of indium, low deposition efficiency,[1] high cost of the sputter deposition process and brittleness. Much effort has been made in recent decades to find materials to replace ITO in transparent conductors. Emerging transparent electrodes include thin films of indium free metal oxides,[2] polymers,[3-5] metallic nanostructures,[6-10] carbon nanotubes (CNTs)[11-15] and, recently, graphene.[16-20]

A number of alternative metal oxides have been studied, *e.g.*, aluminum- and gallium- doped zinc oxide. Although those materials are indium free, a sputtering process is still required for the film fabrication and the drawbacks of high cost and brittleness remain. And new problems have been found in the indium-free materials, such as the instability of aluminum doping.[2] Various doped conducting polymers (*e.g.*, polypyrrole, polyaniline, polythiophene) have also been developed.[3-5, 21] Their limited electrical conductivities and unstable doping state, however, hinder their practical applications.[5, 21]

Thin-films of CNT network have thus been developed to serve as transparent electrodes due to their good transparency and conductivity.[22, 23] A major issue that hinders the adoption CNT network to replace ITO is the resistance caused by tube-tube junctions existence in the network of CNT film.[24-26] Although the DC conductivity (σ_{DC}) of a single CNT has been reported as high as 200000 S cm^{-1} with mobility > 100000 cm^2 Vs^{-1},[27, 28] un-doped CNT random network films have not exceeded 6600 S cm^{-1} conductivity[12] and of order 1-10 cm^2 Vs^{-1} mobility.[29] The best result to date for CNT transparent electrode is R_s = 60 Ω sq^{-1} and T = 91%; the nanotubes in this study were doped by super acid.[14] However, studies on CNT-dopant systems have shown limited stability of the doping effects in air and under thermal loading.[30] Thus, although CNTs offer many advantages, such as low cost and superior adaptability to flexible substrates, it remains difficult to apply CNT networks as a replacement for ITO in transparent electrodes.

Metal thin films (< 10 nm thick) have also been explored as transparent conductors. But the conductivity of metallic films drops dramatically when their thickness is smaller than the mean free path length of charge carriers and because of discontinuity commonly resulting from the deposition process.[31] Random networks of long metallic nanowires with small diameter have also been explored for transparent electrodes. As reported by De *et al.*, sheet resistance of 13 Ω sq^{-1} at transmittance (T) 85% is achieved by transferring a 107 nm-thick Ag nanowire film onto PET substrate.[8] A recent study shows that the addition of 6 wt% SWNTs decreases the sheet resistance of hybrid network electrodes (28.9 Ω sq^{-1}) to one-fourth that of the pure Ag nanowire network electrodes (132 Ω sq^{-1}), since the added SWNTs improve the conductive path percolation in the Ag nanowire network.[32] Another idea for enhancing transparency while keeping conductivity high is to use metal grids on transparent substrates. Metal grids as transparent conductors have been investigated and fabricated by lithography,[6, 33] and roll-to-roll printing[34] and self-assembly of metallic nanoparticles.[35-37] The empty areas of these grids transmit light but compromise the continuous electrical interface with other functional components in the device. In addition, the metallic nanostructure based electrodes (both networks of metallic nanowires and metal grids) exhibit local discontinuities in the sheet resistance which are problematic for many applications. For instance, the excitons generated in the active layer of a solar cell may be quenched before reaching the nearest conduction path (this effect dominates if the size of the void areas in the metal grid or the percolating network of metallic nanowires is larger than the charge diffusion length).[9, 21] In an effort to tackle this issue, Ghosh *et al*. have deposited a 2 nm thick nickel film on top of a copper grid to yield a continuous electrode.[6] A sheet resistance of 6.5 Ω sq^{-1} at

transmittance ~75% is achieved. More recently, Zhu *et al.* demonstrated a method to prepare hybrid films of graphene and photolithography-produced metal grids.[38] At T = 79%, sheet resistances of ~18 Ω sq^{-1} and ~8 Ω sq^{-1} were achieved for, respectively, graphene-aluminum grid and graphene-copper grid hybrid films on flexible substrates.[38] Compared to ultra-thin metal films, graphene is more transparent, more flexible, and more chemically inert. However, the high cost and limited area of CVD-grown graphene make it still not an ideal solution for commercial applications.

In this work, we demonstrate hybrid transparent conductor films produced by solution coating a thin-film network of single-walled CNTs (SWNTs) onto a silver (Ag) network self-assembled from nanoparticle on polyethylene-terephthalate (PET) substrate. These hybrid films (measuring up to 16 cm by 12 cm) exhibit low sheet resistance and high transparency (R_s ~5.8 Ω sq^{-1}, T = 83.7% at λ = 550 nm), high stability in ambient conditions, and excellent bendability. And the simple solution-based coating method makes it scalable to the large-scale low-cost production necessary for widespread applications. We also demonstrate a proof-of-concept application of this hybrid transparent film for photovoltaics. Specifically, with an additional electrochemically deposited ZnO layer, the resulting ZnO-SWNT-Ag-PET film exhibits remarkable enhancement of photocurrent efficiency compared to the SWNT-free ZnO-Ag-PET film.

Results and discussion

Figure 1A schematically illustrates the SWNT-Ag hybrid electrode. The PET film with patterned Ag nanoparticles is commercially available (Cima NanoTech); it is made by large-scale solution-based self-assembly of Ag nanoparticles. Figure 1B and 1C show low magnification scanning electron microscopy (SEM) images of the Ag-PET film without and with SWNT network, respectively(no Pt coating before SEM imaging). The size of the empty areas bounded by the Ag lines ranges from 100 µm to 500 µm. For the sample without SWNT network, the empty area (without Ag) is PET substrate only. As PET is non-conductive, these areas were heated and deformed (bulged) under electron beam. The image of Ag-PET with SWNT network on top is absent of this problem and appears clearer because the highly conductive nature of SWNT network. SEM high magnification imagery shows that the Ag network is composed of densely packed Ag nanoparticles (Figure 1D). The CNTs were P2-SWNTs purchased from Carbon Solutions, and used as received. Immersion of Ag-PET film into a dispersion of these SWNTs results in deposition of a network of SWNTs on the Ag-PET surface. To enhance SWNT/substrate adhesion, the Ag-PET film was treated with (3-Aminopropyl)triethoxysilane (APTES) prior to immersion in the SWNT dispersion. In order to avoid deposition of SWNTs on the underside of the Ag-PET film, which would reduce transparency without improving the conductivity of the film, the underside was protected with a sacrificial layer of plain PET film during all surface treatment steps. The sacrificial layer can be easily removed after SWNT deposition. The SWNT network on top of the packed Ag nanoparticles is evident in the high magnification image (Figure 1E). The SWNT network thin film at the empty area is shown in

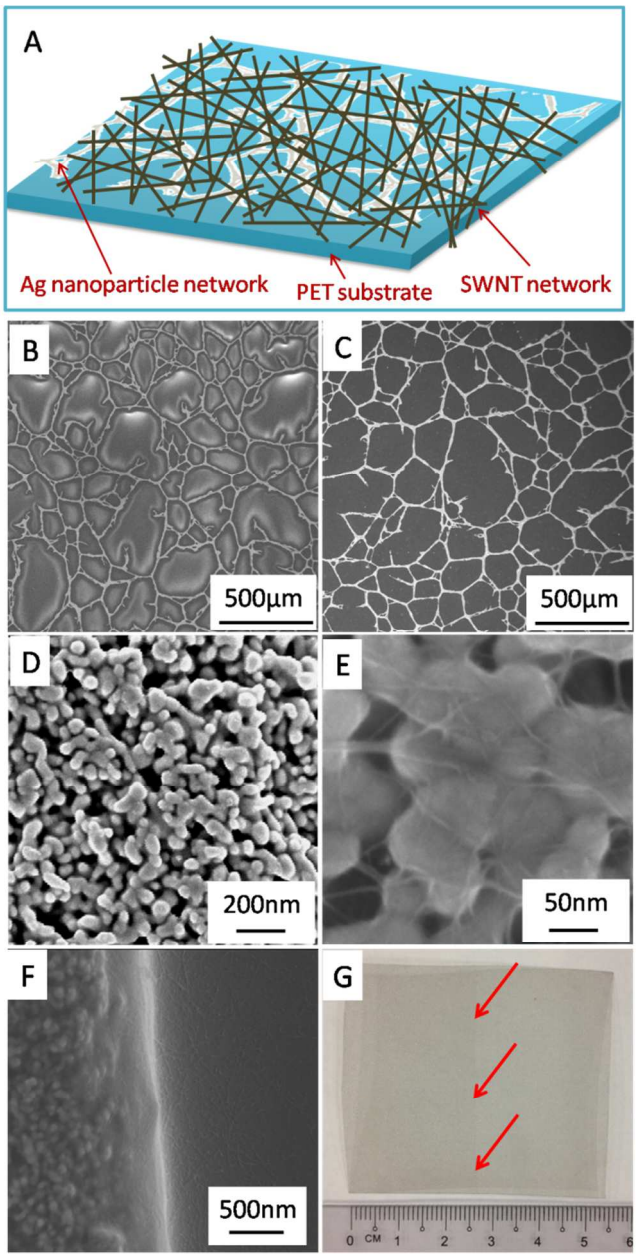

Fig. 1A) Schematic illustration of SWNTs-Ag-PET hybrid transparent electrodes (not to scale). The light grey network in the figure represents the Ag nanoparticle network self-assembled on the PET substrate. B) and C) show low magnification SEM images of Ag-PET films without and with SWNT network. The SWNT network covered areas are darker and flat in C). D) High magnification SEM image of Ag nanoparticles, assembled into part of a network gridline. E) High magnification SEM image of SWNT-Ag-PET hybrid film, showing the network of SWNTs on top of a portion of an Ag network gridline. F) SEM image of SWNT-Ag-PET hybrid film, which shows that the SWNT network adheres and follows the topology of the Ag-PET substrate very well. G) A photograph of Ag-PET film with (left) and without (right) a SWNT network. The red arrows show the boundary between the regions with/without CNT thin film. The size of the SWNT-Ag-PET sample is 5.5 cm × 5 cm.

Figure S1 (Supporting Information).The SEM image in Figure 1F shows that the SWNT network conforms to the vertical relief of the Ag conductor and the PET substrate. Figure 1G shows the gross appearance of a 5.5 cm × 5 cm SWNTs-Ag-PET film. The right side of this film was covered to prevent SWNT deposition;

and the boundary between the regions with/without SWNTs, which differ only slightly in transparency, is marked in the image. Large-sized hybrid films can be fabricated (Figure S2, Supporting Information). The size of hybrid film need not be constrained by the dimensions of a container of SWNTs dispersion; the SWNT film may be deposited by printing or spray-coating for effective large scale manufacture.

The unpredictable character of circuit continuity and conductive percolation through the Ag network of the Ag-PET film is reflected in large variations in sheet resistance measured by a four-point probe station. As shown in Figure 2A, the majority of measurements at different locations show low or no conductance. The three different groups of R_s value are due to the different locations measured. The four-point probe measurement is illustrated in Figure S3 (Supporting Information). Low sheet resistance is obtained when all the 4 probes are located on the main stem of Ag grids while high sheet resistance results when any of the probes is located in the empty area. The intermediate resistance is resulted when probe 2 or 3 is on a branch of the Ag-grids (highlighted by the circles in Figure S3-B, Supporting Information). In the third situation, the circuit is still closed, but the voltage measured between Probe 2 and Probe 3 will be much smaller because most of the current flows through the main stem rather than the branches. In contrast, SWNT-Ag-PET hybrid films provide homogeneous and low sheet resistance (5.8±1.1 Ω sq^{-1}, n=50) at all measured points. The sheet resistance of the SWNT network itself (on PET substrate) is high (13.7±1.9 kΩ sq^{-1}, n=50) (Figure 2A). Therefore, the high conductivity of SWNT-Ag-PET film is mainly due to the Ag network. For comparison of SWNT-Ag-PET with other potential advanced conductive materials as the deposited conductivity enhancing layer, CVD-grown graphene and 99% metallic-enriched SWNTs (met-SWNT), were also applied on top of the Ag-PET substrates (experimental details and results in Supporting Information). As shown in Figure S4-S7 (supporting Information), the graphene and met-SWNT thin-film hybridized electrodes give similar performance in terms of sheet resistivity, transparency, and bendability. However, from the standpoint of cost, the un-sorted SWNTs are much less expensive than the other two materials. Another cheap alternative material would be reduced graphene oxide (GO).[39] Additional processing is required to reduce deposited GO to conductive reduced GO, so that un-sorted SWNT deposition appears superior even to this alternative from the standpoint of process simplicity.

In addition to bridging the discontinuities in the Ag network conductive paths, the CNT network improves the homogeneity of the electrode and also modestly increases the electrode conductivity by electrically bridging the voids in the conductive Ag network. The deposited CNT network slightly decreases the optical transmittance, from 85.4% to 83.7% at 550 nm wavelength (Figure 2B).

SWNT-Ag-PET film is flexible and is durable under repeated bending stress. After 1000 cycles bending (bending radius = 8 mm), the sheet resistivity of the hybrid film remains below 10 Ω sq^{-1} (Figure 2C), while that of thin ITO films was reported to increase irreversibly by almost 2 orders of magnitude after <200 bending cycles.[40] SEM images show the excellent adhesion of

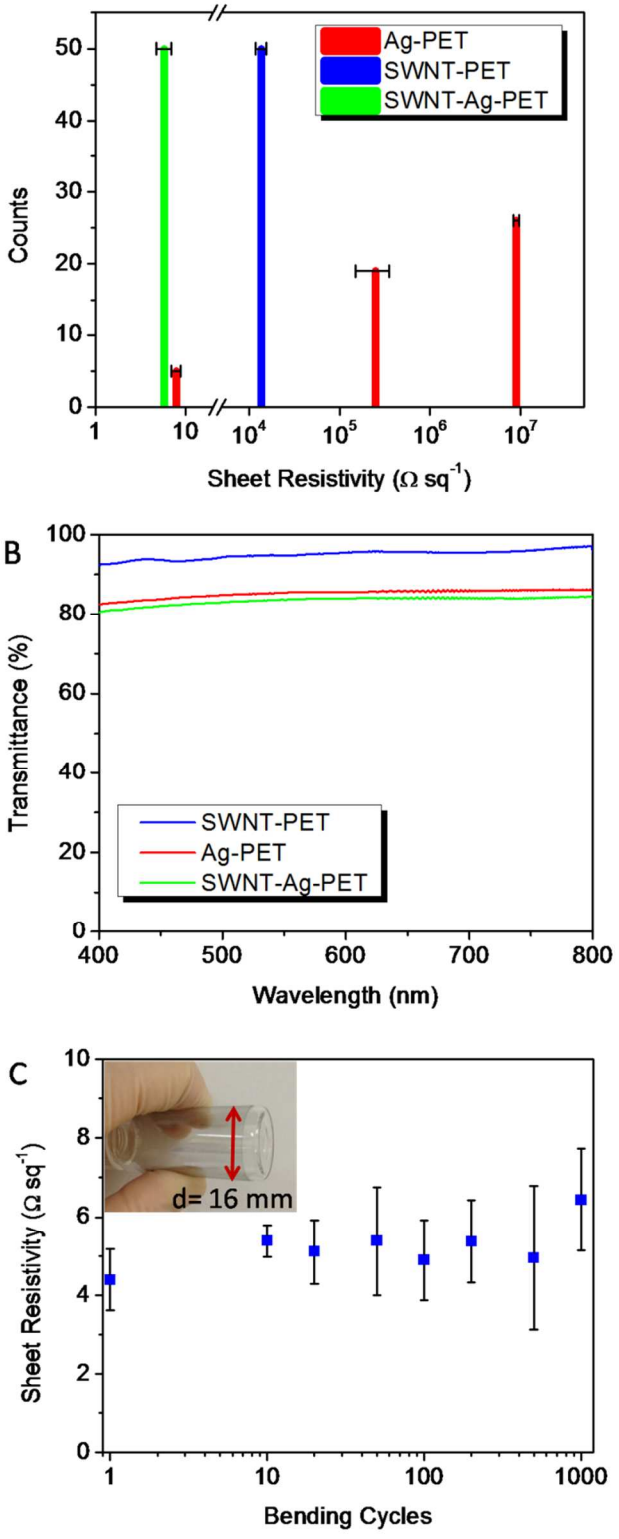

Fig. 2A) Sheet resistance of Ag-PET film (red), thin film of SWNT network (blue), and SWNT-Ag-PET hybrid film (green). 50 points were measured for each sample. B) Transmittance of SWNT-PET film (blue curve), Ag-PET film without (red curve) and with (green curve) deposited SWNT network. C) Flexibility test of the SWNT-Ag-PET film. The plot shows the sheet resistivity of the SWNT-Ag-PET film,as a function of bending cycles, up to 1000 cycles. Inset shows the extent to which the SWNT-Ag-PET film was bent in the flexibility test.

SWNT thin film to the Ag-PET substrate even after 1000 cycles of bending (Figure S8). No mechanical degradation is observed for either the Ag nanoparticles or thin film of SWNT network after the bending test (Figure S8, Supporting Information). The SWNT-Ag-PET hybrid films are quite stable, showing no difference in sheet resistance, compared with freshly-prepared samples, after >1 month exposure to ambient conditions.

We compare the sheet resistance and transmittance performance metrics of our hybrid film with other transparent conductors in Table S1. However, sheet resistances obtained at different transmission levels cannot be directly compared. A useful figure of merit for comparison of material properties in this situation is the ratio $\sigma_{DC}/\sigma_{Op}(\lambda)$, where $\sigma_{Op}(\lambda)$ is the optical conductivity at wavelength λ and σ_{DC} is the DC conductivity of the film. Higher values of this figure of merit imply better performance. This ratio can be derived from the measured transmittance T and sheet resistance R_s through the relation[8, 21]

$$T(\lambda) = \left(1 + \frac{188.5}{R_s}\frac{\sigma_{Op}(\lambda)}{\sigma_{DC}}\right)^{-2} \quad (1)$$

As shown in Table S1, for commonly used commercial ITO with R_s = 30-80 Ω sq^{-1} at T = 90%, σ_{DC}/σ_{Op} is calculated to be ~50-120 (No. 4 in Table S1).While the best results for doped graphene and carbon nanotube films are ~120 and ~60respectively (No. 13 and 6 in Table S1).[14, 16] The σ_{DC}/σ_{Op} of our SWNT-Ag-PET film is ~350 which is significantly higher than that of ITO, doped CNTs and graphene. The performance of our hybrid films is comparable to that of graphene-gold grid films demonstrated by Zhu *et al.* (No.16 in Table S1, R_s= 4±1Ω sq^{-1}, T = 79%, σ_{DC}/σ_{Op} ~377).[38] However, these graphene-gold grid films were made on rigid substrates and their fabrication requires costly photolithography and thermal evaporation processes. Using similar technique, the same authors also fabricated CVD graphene-aluminum grid films and CVD graphene-copper grid films on both glass and PET substrates. But these films showed poorer performance than our SWNT-Ag-PET film, with lower σ_{DC}/σ_{Op} of 65-188 (R_s= 18±9 Ω sq^{-1} for graphene-Al hybrid; and R_s= 8±3 Ω sq^{-1} for graphene-Cu hybrid; both at T = 79% and on PET substrates).

To demonstrate a potential application of the SWNT-Ag-PET hybrid film as photovoltaic electrode, we electrochemically deposited ZnO nanoplates on SWNT-Ag-PET electrode, and on as received Ag-PET as a control, and used the semi-transparent ZnO-decorated electrodes as photoanodes of photo-electrochemical cells. ZnO, a n-type semiconducting metal oxide, has been intensively studied for application in dye-sensitized solar cells due to its wide band gap and high electron mobility.[41] The SEM image at low magnification (Figure 3A) shows that the SWNT-Ag-PET hybrid electrode is fully and uniformly covered with ZnO nanoplates. Higher magnification SEM (Figure 3B) shows the rose-like morphology of the ZnO nanoplates. The XRD pattern confirms the crystallinity of ZnO nanoplates (Figure 3E). In contrast, ZnO nanostructures are not observed in the SWNT-free Ag-PET films (Figure 3C&D). In addition, Ag wires appear to be degraded to some extent due to the electrochemical migration of Ag under electrical field.[42] The problem of Ag migration is relieved for the SWNT-Ag-PET sample because of the protection offered by the well-adhered SWNT thin film.[39, 42] The photocurrent responses of the ZnO-decorated electrodes are shown in Figure 3F. Upon excitation with visible light, a weak current (~ 1 μA cm^{-2}) was observed on the SWNT-free ZnO-Ag-PET anode, while a remarkably enhanced current (13-16 μA cm^{-2}) was generated with the ZnO-SWNT-Ag-PET anode. Although the current is low, compared to that produced by complicated heterostructured photoanodes reported recently,[43] the significant improvement of photocurrent efficiency with the CNT thin film is clearly demonstrated in this experiment, as a concept proof. The CNT network enhances the photocurrent in two ways: 1) during the electrochemical fabrication process, the CNT network bridges the Ag grid to make the hybrid electrode homogeneously conductive, permitting homogeneous deposition of ZnO nanoplates to fully cover the hybrid electrode; 2) in use, the excellent electron-accepting ability of the CNTs facilitates charge collection and transport.[44, 45]

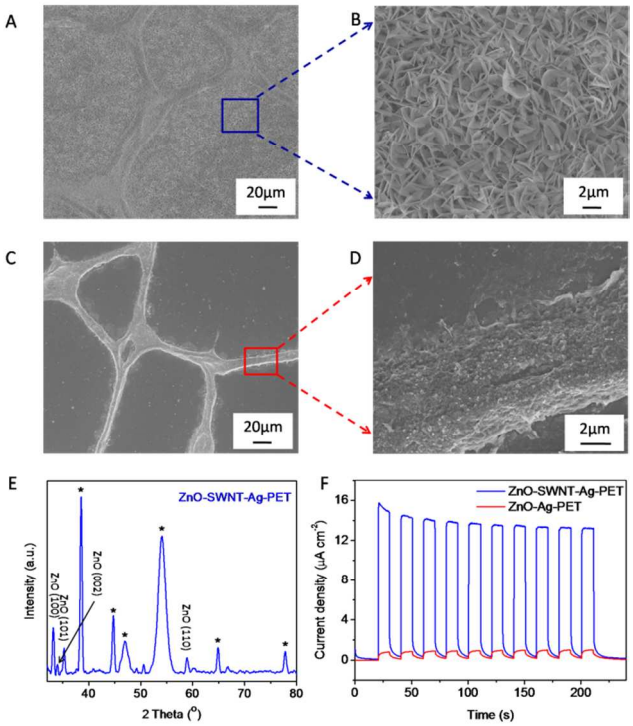

Figure 3. A) SEM image of ZnO-SWNT-Ag-PET at low magnification, showing the uniformly deposition of ZnO nanosructure on SWNT thin film, with or without Ag grids. B) Zoom-in SEM image of the area in blue square, showing the rose-like morphology of the ZnO nanostructures. C) SEM image of ZnO-Ag-PET at low magnification, showing no ZnO nanostructure deposited. D) Zoom-in SEM image of the area in red square. E) XRD pattern of ZnO-SWNT-Ag-PET photoanode. The peaks marked with * are from Ag nanoparticles. F) Amperometric *I-t* curve of ZnO-SWNT-Ag-PET photoanode (blue curve) and ZnO-Ag-PET photoanode (red curve).

Conclusions

In summary, we have demonstrated a solution-based method for fabrication of hybrid transparent and flexible electrodes which combines Ag nanoparticle networks and thin films of SWNT network. This type of electrode can be simply and scalably fabricated at low-cost. Its outstanding performance (R_s ~5.8 Ω sq^{-}

[1], T = 83.7% at λ = 550 nm, σ_{DC}/σ_{Op} ~350) together with its robustness and flexibility suggest a wide range of potential industrial and commercial applications.

Acknowledgements

We thank Cima NanoTech for providing the Ag-PET films. This work was supported by a Competitive Research Program grant from the Singapore National Research Foundation (NRF-CRP2–2007-02). J. Wang acknowledges the support of Nanyang Technological University through a Research Scholarship.

Notes and references

School of Chemical and Biomedical Engineering, Nanyang Technological University, Singapore 637459, Singapore. Tel: (65) 6790 6064, Fax: (65) 6794 7553, Email: mbechan@ntu.edu.sg, chenpeng@ntu.edu.sg

† Electronic Supplementary Information (ESI) available: Experimental details, performance of graphene-Ag hybrid and met-SWNT-Ag hybrid films. See DOI: 10.1039/b000000x/

1. M. A. Green, *Prog. Photovoltaics*, 2009, **17**, 347-359.
2. T. Minami, *Thin Solid Films*, 2008, **516**, 1314-1321.
3. A. Elschner and W. Lovenich, *MRS Bull.*, 2011, **36**, 794-798.
4. S. A. Carter, M. Angelopoulos, S. Karg, P. J. Brock and J. C. Scott, *Appl. Phys. Lett.*, 1997, **70**, 2067-2069.
5. S. Kirchmeyer and K. Reuter, *J. Mater. Chem.*, 2005, **15**, 2077-2088.
6. D. S. Ghosh, T. L. Chen and V. Pruneri, *Appl. Phys. Lett.*, 2010, **96**, 041109.
7. D. S. Ghosh, T. L. Chen and V. Pruneri, *Appl. Phys. Lett.*, 2010, **96**, 091106.
8. S. De, T. M. Higgins, P. E. Lyons, E. M. Doherty, P. N. Nirmalraj, W. J. Blau, J. J. Boland and J. N. Coleman, *ACS Nano*, 2009, **3**, 1767-1774.
9. L. B. Hu, H. S. Kim, J. Y. Lee, P. Peumans and Y. Cui, *ACS Nano*, 2010, **4**, 2955-2963.
10. L. B. Hu, H. Wu and Y. Cui, *MRS Bull.*, 2011, **36**, 760-765.
11. H. Z. Geng, K. K. Kim, K. P. So, Y. S. Lee, Y. Chang and Y. H. Lee, *J. Am. Chem. Soc.*, 2007, **129**, 7758-7759.
12. Z. C. Wu, Z. H. Chen, X. Du, J. M. Logan, J. Sippel, M. Nikolou, K. Kamaras, J. R. Reynolds, D. B. Tanner, A. F. Hebard and A. G. Rinzler, *Science*, 2004, **305**, 1273-1276.
13. L. B. Hu, D. S. Hecht and G. Gruner, *Chem. Rev.*, 2010, **110**, 5790-5844.
14. D. S. Hecht, A. M. Heintz, R. Lee, L. B. Hu, B. Moore, C. Cucksey and S. Risser, *Nanotechnology*, 2011, **22**, 075201.
15. H. Tantang, J. Y. Ong, C. L. Loh, X. C. Dong, P. Chen, Y. Chen, X. Hu, L. P. Tan and L. J. Li, *Carbon*, 2009, **47**, 1867-1870.
16. S. Bae, H. Kim, Y. Lee, X. F. Xu, J. S. Park, Y. Zheng, J. Balakrishnan, T. Lei, H. R. Kim, Y. I. Song, Y. J. Kim, K. S. Kim, B. Ozyilmaz, J. H. Ahn, B. H. Hong and S. Iijima, *Nat. Nanotechnol.*, 2010, **5**, 574-578.
17. F. Gunes, H. J. Shin, C. Biswas, G. H. Han, E. S. Kim, S. J. Chae, J. Y. Choi and Y. H. Lee, *ACS Nano*, 2010, **4**, 4595-4600.
18. K. K. Kim, A. Reina, Y. M. Shi, H. Park, L. J. Li, Y. H. Lee and J. Kong, *Nanotechnology*, 2010, **21**, 285205.
19. X. S. Li, Y. W. Zhu, W. W. Cai, M. Borysiak, B. Y. Han, D. Chen, R. D. Piner, L. Colombo and R. S. Ruoff, *Nano Lett.*, 2009, **9**, 4359-4363.
20. J. Wang, X. C. Dong, R. Xu, S. Z. Li, P. Chen and M. B. Chan-Park, *Nanoscale*, 2012, **4**, 3055-3059.
21. D. S. Hecht, L. B. Hu and G. Irvin, *Adv. Mater.*, 2011, **23**, 1482-1513.
22. M. W. Rowell, M. A. Topinka, M. D. McGehee, H. J. Prall, G. Dennler, N. S. Sariciftci, L. B. Hu and G. Gruner, *Appl. Phys. Lett.*, 2006, **88**.
23. D. H. Zhang, K. Ryu, X. L. Liu, E. Polikarpov, J. Ly, M. E. Tompson and C. W. Zhou, *Nano Lett.*, 2006, **6**, 1880-1886.
24. M. S. Fuhrer, J. Nygard, L. Shih, M. Forero, Y. G. Yoon, M. S. C. Mazzoni, H. J. Choi, J. Ihm, S. G. Louie, A. Zettl and P. L. McEuen, *Science*, 2000, **288**, 494-497.
25. P. N. Nirmalraj, P. E. Lyons, S. De, J. N. Coleman and J. J. Boland, *Nano Lett.*, 2009, **9**, 3890-3895.
26. J. L. Blackburn, T. M. Barnes, M. C. Beard, Y. H. Kim, R. C. Tenent, T. J. McDonald, B. To, T. J. Coutts and M. J. Heben, *ACS Nano*, 2008, **2**, 1266-1274.
27. T. W. Ebbesen, H. J. Lezec, H. Hiura, J. W. Bennett, H. F. Ghaemi and T. Thio, *Nature*, 1996, **382**, 54-56.
28. T. Durkop, S. A. Getty, E. Cobas and M. S. Fuhrer, *Nano Lett.*, 2004, **4**, 35-39.
29. Q. Cao, S. H. Hur, Z. T. Zhu, Y. G. Sun, C. J. Wang, M. A. Meitl, M. Shim and J. A. Rogers, *Adv. Mater.*, 2006, **18**, 304-309.
30. R. Jackson, B. Domercq, R. Jain, B. Kippelen and S. Graham, *Adv. Funct. Mater.*, 2008, **18**, 2548-2554.
31. E. H. Sondheimer, *Advances in Physics*, 1952, **1**, 1-42.
32. T. Tokuno, M. Nogi, J. Jiu and K. Suganuma, *Nanoscale Research Letters*, 2012, **7**, 1-7.
33. M. G. Kang and L. J. Guo, *Adv. Mater.*, 2007, **19**, 1391-1396.
34. J. Woerle and H. Rost, *MRS Bull.*, 2011, **36**, 789-793.
35. *US Pat.,* 7601406, 2005.
36. A. Morag, L. Philosof-Mazor, R. Volinsky, E. Mentovich, S. Richter and R. Jelinek, *Adv. Mater.*, 2011, **23**, 4327-4331.
37. *US Pat.,* 8105472, 2012.
38. Y. Zhu, Z. Z. Sun, Z. Yan, Z. Jin and J. M. Tour, *ACS Nano*, 2011, **5**, 6472-6479.
39. I. N. Kholmanov, S. H. Domingues, H. Chou, X. Wang, C. Tan, J.-Y. Kim, H. Li, R. Piner, A. J. G. Zarbin and R. S. Ruoff, *ACS Nano*, 2013, **7**, 1811-1816.
40. S. De, P. E. Lyons, S. Sorel, E. M. Doherty, P. J. King, W. J. Blau, P. N. Nirmalraj, J. J. Boland, V. Scardaci, J. Joimel and J. N. Coleman, *ACS Nano*, 2009, **3**, 714-720.
41. Q. F. Zhang, C. S. Dandeneau, X. Y. Zhou and G. Z. Cao, *Adv. Mater.*, 2009, **21**, 4087-4108.
42. L. Yi and C. P. Wong, *Appl. Phys. Lett.*, 2006, **89**, 112112.
43. Z. Y. Yin, Z. Wang, Y. P. Du, X. Y. Qi, Y. Z. Huang, C. Xue and H. Zhang, *Adv. Mater.*, 2012, **24**, 5374-5378.
44. F. Vietmeyer, B. Seger and P. V. Kamat, *Adv. Mater.*, 2007, **19**, 2935-2940.
45. A. Kongkanand, R. Martínez Domínguez and P. V. Kamat, *Nano Lett.*, 2007, **7**, 676-680.